Nanoscale

Accepted Manuscript

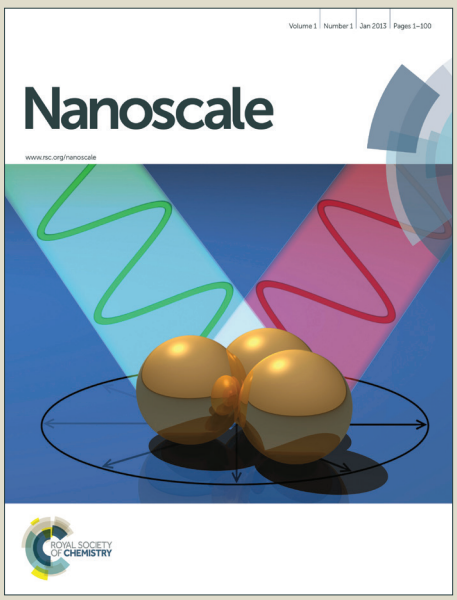

ROYAL SOCIETY OF CHEMISTRY

www.rsc.org/nanoscale

Fano Resonances in Three-Dimensional Dual Cut-wire Pairs

Xingzhan Wei,[1]* Matteo Altissimo,[2] Timothy J. Davis,[2,3] and Paul Mulvaney[1]*

[1]School of Chemistry and Bio21 Institute, University of Melbourne, Parkville, Victoria, 3010, Australia

[2]Melbourne Centre for Nanofabrication, ANFF, 151 Wellington Road, Clayton, Victoria 3168, Australia

[3]CSIRO, Materials Science and Engineering, Private Bag 33, Clayton, VIC, 3168, Australia

E-mail: xiwei@unimelb.edu.au; mulvaney@unimelb.edu.au

*To whom correspondence should be addressed

KEYWORDS: Fano resonance, surface plasmon, coupling, nanofabrication, dark mode, retardation effect

ABSTRACT: This paper presents an experimental demonstration of pronounced Fano resonances in a remarkably simple, three-dimensional (3D) plasmonic system, composed of two groups of paired cut-wires with different sizes. Theoretical calculations using the Finite Element Method, which are in good agreement with the experiment, are provided to describe the Fano behaviour. The dependence of the Fano line shapes on the separation and offset between the two cut-wire pair units is quantitatively analyzed. The generation of Fano resonances in such nanostructures presents clear advantages over current 3D structures, because of their easier fabrication, and because the optical spectra can be easily and predictably tuned.

Fano resonances can be constructed in metallic nanostructures by exploiting the interference between a broad superradiant (bright) mode and a narrow subradiant (dark) mode that are spectrally overlapping. Because these resonances exhibit steep, asymmetric profiles, plasmonic Fano resonances may yield applications in lasing [1], nonlinear optics [2, 3], low loss metamaterials [4-6], subwavelength waveguides [7-9] and sensors [10, 11]. Therefore, it is not surprising that various plasmonic structures have been proposed and demonstrated as candidates for generating Fano resonances. Two-dimensional planar geometries including nanoshells with asymmetric cores [12], "dolmen" structures [13-15], mismatched nanoparticle pairs [16], coupled ring-disk structures [13, 17, 18], self-assembled tetramer clusters [19], and symmetric or asymmetric heptamers [20-23] have all been shown to support Fano resonances. Intriguing electromagnetic interaction mechanisms are also expected in ***three*** dimensions; for example a nanoplasmonic analogue consisted of two functional layers, namely a gold bar stacked above two symmetric gold wires, has been experimentally demonstrated to exhibit electromagnetically induced transparency [24]. Furthermore, a 3D plasmon ruler composed of three functional layers in close proximity [25, 26] has been realized in order to create sharp spectral features, and this structure exhibits double transparency, which is extremely promising in the fields of biology and soft materials science. However, due to the complex design, the fabrication of these 3D structures is time-consuming and involves multiple, complicated steps: for instance, surface planarization, precise alignment with registration marks and two or three electron beam exposures.

Herein, we demonstrate that Fano resonances can be observed in a remarkably simple 3D plasmonic system consisting of two groups of paired asymmetric cut-wires. As the structures of the top and bottom functional layers are designed to be the same in this two-functional-layer

(TFL) system, this cluster can be fabricated with just one electron beam exposure and one standard lift-off process. The experimental data demonstrate that the Fano resonance energies depend strongly on the lengths of the cut-wire pairs. We have calculated the scattering spectra using the Finite Element Method (Comsol), and show that one can also modulate the resonance energy by adjusting the geometrical parameters, such as the gap and offset between the two cut-wire pairs. Moreover, this Fano resonance cluster acts as a 3D capacitor, which is capable of storing optical energy. We believe the combination of easy modulation, high electric field enhancement, and simple fabrication, renders this 3D plasmonic system ideal for a wider range of nanotechnology applications, such as thin film solar cells and novel sensors with high sensitivity in three dimensions.

A simple metallic cut-wire is regarded as an elementary plasmonic oscillator whose localized surface plasmon resonances are determined by its size and the refractive index of surrounding environment. It is interesting to modify the resonance behaviour via near-field coupling. This can be achieved by placing other nanoparticles in close proximity, which sometimes leads to the formation of dark modes. When four cut-wires with the same size are sufficiently closely spaced, they comprise a fully symmetric 3D quadrumer, as shown in Fig 1a. This system supports one coupled bright mode in which the four dipole modes from the individual cut-wires interact in phase. Furthermore, there are several dark modes with zero net dipole moment, which do not contribute to the scattering spectra. The dark modes cannot be excited by normally incident plane waves, nor can they directly interact with the bright modes. However, symmetry breaking is an effective mechanism for activating the coupling between the dark modes and the bright modes. This can be achieved for example by making one cut-wire pair shorter than the other one. In order to demonstrate the effect of symmetry breaking, we compare

the scattering spectra of the symmetric and asymmetric quadrumers, as shown in the top picture of Fig. 1b. The spectrum of the symmetric quadrumer (black curve) exhibits a Lorentzian line shape with a peak at around 750 nm. In contrast, the red curve denotes the scattering spectrum of the asymmetric quadrumer, which exhibits a steep Fano resonance profile and a clear dip at around 765 nm.

The surface charge density plots at the interesting wavelengths marked as (i) and (ii) are shown in Fig. 1c. The symmetric quadrumer exhibits an anti-bonding mode, in which the dipole modes of the four cut-wires hybridize in-phase and interact repulsively, leading to the suppression of near-field intensity. Especially at the locations in the middle of these two pairs, the values of $|E|$ approach zero, as shown in the top picture of Fig. 1d. In the case of the asymmetric quadrumer, the dipole moments of the long and short stacked pairs are out-of-phase, and the near-field interaction becomes attractive. Thus, highly enhanced electric fields are formed at the gap locations, as shown in the bottom picture of Fig. 1d. This effect is ascribed to formation of a Fano resonance due to symmetry breaking. Specifically, destructive interference occurs between the two excitation pathways of the bright mode: direct excitation ($|I\rangle \rightarrow |B\rangle$), and indirect excitation ($|I\rangle \rightarrow |B\rangle \rightarrow |D\rangle \rightarrow |B\rangle$) due to the interaction of the bright mode with the dark mode, where $|I\rangle$ represents a continuum of incident photons while $|B\rangle$ and $|D\rangle$ denote the bright and dark mode states, respectively [19]. This destructive interference leads to a suppression of radiative damping, and thus this mode stores a large amount of electromagnetic energy. The near-field intensity of the asymmetric quadrumer at the Fano resonance wavelength is nearly 3 times higher than the maximum value of the symmetric quadrumer, as shown in the bottom picture of Fig. 1b. Note that this is an integrated value over the whole near-field region around the quadrumer, and we believe this value could be greatly increased at some specific "hot-spot"

locations. It also should be noted that the entire Fano resonance system acts as a 3D cavity, which produces coupling in both the horizontal and vertical planes. Due to the coupling between the top and bottom layers, the intensities inside the cavity are obviously stronger than outside the cavity. The relevant electric field intensity images at different vertical planes are shown in Figure S1 of the Supporting Information. These characteristics are quite different to those observed in the above-mentioned 2D Fano resonance structures [12-23], in which the electromagnetic interaction occurs mainly in the planar horizontal plane, and consequently, the electric fields decay rapidly in the vertical direction.

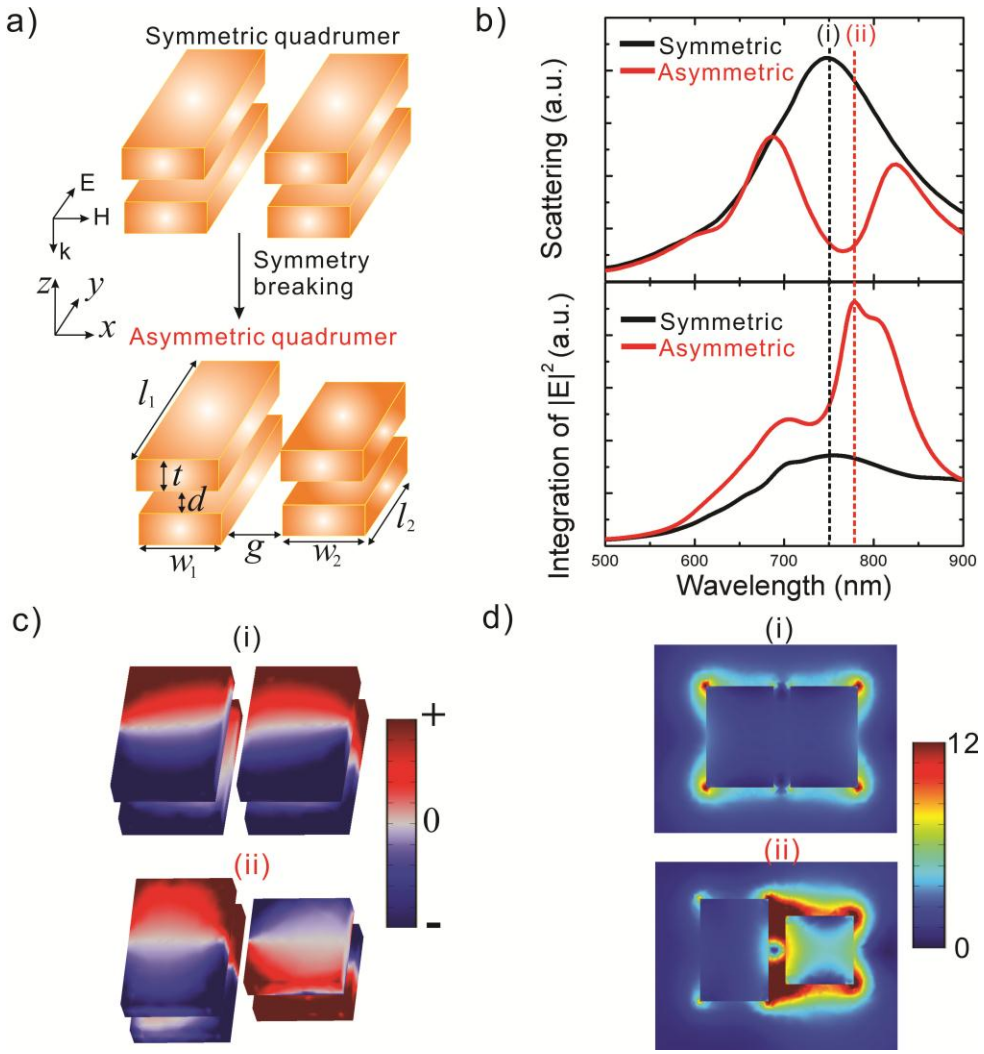

Fig. 1 (a) Schematic illustration of Fano resonance behaviour produced by symmetry breaking. The normally incident light is polarized along the major axis of the cut wires. (b) Calculated scattering spectra (top picture) and integration of the near-field intensity ($|E|^2$) (bottom picture) as a function of wavelength for the symmetric and asymmetric quadrumers. The Fano minimum is at 765 nm. The optical properties of the structures were modelled using the Finite Element Method (Comsol). The optical constants of gold were taken from Johnson and Christy [28]. All structures are embedded in an effective dielectric medium with a refractive index of 1.25. The integration of the near-field intensity values ($|E|^2$) was done in the near-field space around the quadrumer within 20 nm. The peaks in the near-field intensities are denoted by black (marked as black (i) and red (ii) dashed lines, respectively. (c) Surface charge density plots at the interesting wavelengths are indicated by (i) and (ii). For the symmetric quadrumer, surface charges on every cut-wire oscillate in phase, resulting in constructive interference of their radiated fields. For symmetry-broken clusters, the dipole moments of the long and short pairs oscillate in opposite directions, resulting in destructive interference of their radiated fields. (d) 2D electric field intensity enhancement plots at the central plane of the top layer (z = 20 nm, as indicated in Figure S1(a) of the Supporting Information). For the symmetric quadrumer: $l_1 = l_2 = 120$ nm, $w_1 = w_2 = 80$ nm, $t = 20$ nm, and $g = 20$ nm. For the asymmetric quadrumer: $l_1 = 120$ nm, $l_2 = 80$ nm, $w_1 = w_2 = 80$ nm, $t = 20$ nm, and $g = 20$ nm.

The fabrication of the TFL structures was achieved via a bilayer lift-off process. The resists used were methyl methacrylate (MMA) EL6 and polymethyl methacrylate (PMMA) A2. After exposure in a Vistec EBPG 5000plusES system, the samples were developed in a solution of methyl isobutyl ketone (MIBK) and isopropyl alcohol (IPA) with a volume ratio of 1:3. Subsequently, titanium (1 nm), Au (20 nm), titanium (1 nm), SiO_2 (20 nm), titanium (1 nm) and Au (20 nm) were deposited layer-by-layer using an electron beam evaporator under tightly geometrical deposition conditions. Finally, the TFL structures were obtained by lift-off.

In order to investigate the evolution of the coupling behaviour, a series of TFL structures with varying lengths was fabricated. Optical spectra were collected with a dark-field microscope (Nikon Ti-S). The white excitation light from a 25 W halogen lamp was focused onto the samples using a Nikon dry dark-field condenser, and collected by a MicroSpec 2150i imaging spectrometer equipped with a thermoelectrically cooled charge-coupled device (CCD, Acton Pixis 1024B Exelon). Polarized scattering spectra were obtained by placing a polarizer (LPVIS 100, Thorlabs) in the incident light path. Images of the fabricated structures were obtained by scanning electron microscopy (Quanta, FEI Co.) in low vacuum mode without a coating of any conducting materials,

as shown in the central column of Figure 2. The lift-off based fabrication procedure results in trapezoidal sidewalls, and the angle with respect to the normal of the substrate was measured to be around 8 degrees, similar to the results of Dolling [27]. In Figure 2, the measured and modelled scattering spectra are shown for a series of cut-wire system with varying lengths. For a symmetric cut-wire pair system (l_2 = 125 nm), we find the scattering spectrum exhibits a dominant peak centred at 753 nm, and the curve slopes toward the red in the experiments. In addition, a tiny dip appears at around 718 nm. We point out that the slope and dip arise from the coupling between incident light and the dark mode, which are both excited at large angles of incidence due to the effect of retardation [29, 30], i.e. because the electric field across the nanostructure is no longer uniform as the angle of incidence becomes large. In order to demonstrate the influence of retardation, we have also modelled the scattering spectra as a function of the angle of incidence (See Figure S2 in the Supporting Information). Note that in the normal incidence case, the scattering spectrum exhibits a symmetric Lorentzian line shape and there is no dip. As the angle increases, the influence of retardation becomes stronger.

Prominent Fano resonances are formed when the length of the right side cut-wire pair (l_2) decreases to 105 nm, and as l_2 gradually decreases, the Fano minima exhibits a noticeable blue-shift. Simulated scattering spectra are presented in the right column of Figure 2, and these show good qualitative agreement with the experimental spectra. The resonance wavelength differences between experiment and modelling might arise from the deviations between the actual and the modelled geometrical dimensions of the cut-wire pairs, or because of the choice of dielectric function for gold. It is worth noting that the Fano minimum at 61^o incidence exhibits a minor blue-shift (about 10 nm) compared to the normal incidence case (see Figure S3 in the Supporting Information). This is because, in the oblique incidence case, the incident retarded field and bright mode both interact with

the dark mode. The excitation pathway can be described by $|I> \rightarrow |B> \xrightarrow{I_{Ret}} |D> \rightarrow |B>$, where I_{Ret} represents the incident field excitation caused by retardation [30]. Thus, the Fano resonance must be excited at higher frequencies than in the normal incidence case, in order to compensate for the extra response due to I_{Ret}. The Fano resonances in the experiment are the combined results, although the retardation effect plays a secondary role in determining the line shape of the spectra. The influence of retardation can be minimized by using near-normal-incidence dark-field microscopy [30].

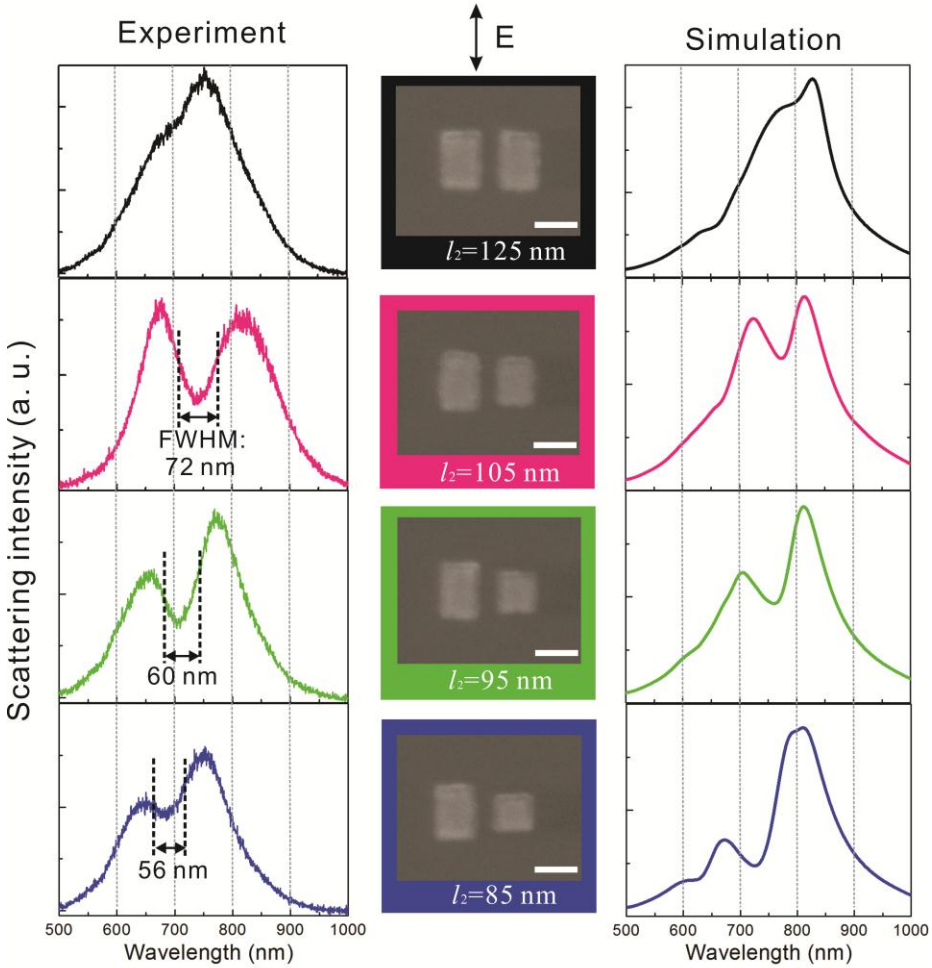

Fig. 2 Normalized scattering spectra as a function of the length of the right hand cut-wire pair (l_2) under oblique incidence (61 °). The polarization direction of the incident light is oriented along the longitudinal direction. Left column: experimental scattering spectra. Middle column: scanning electron microscopy (SEM) images of the corresponding structures, scale bar: 100 nm. Right column: simulated scattering spectra, where the illumination angle and geometry parameters are strictly based on experimental results. l_1 = 125 nm, w_1 = 85 nm, w_2 = 85 nm, t = 20 nm, d = 20 nm and g = 30 nm. The values of l_2 are 125 nm, 105 nm, 95 nm

and 85 nm, respectively, as indicated from the top row to the bottom. The full width half maximum (FWHM) of the Fano resonances are 72 nm, 60 nm, and 56 nm when l_2 = 105 nm, 95 nm and 85 nm, respectively.

The geometrical parameters play a crucial role in the plasmon coupling, and therefore, in the line shape of the Fano resonance spectra. We now analyze the effect of the gap and location of the cut-wire pair on the optical properties in the normal incidence case, where retardation is less important. Figure 3a depicts the optical responses of two cut-wire pairs with different gaps. The Fano minima exhibit a blue-shift and the Fano resonance becomes less pronounced as the gap increases. The influence of a structural offset on the optical response is analyzed in Figure 3b. The displacement of the cut-wire pair along the longitudinal direction causes a considerable blue-shift of the Fano minima. As the offset increases, it generates a weaker Fano resonance. To quantify the resonance coupling, we have fit the calculated spectra using the analytical expressions developed by Gallinet and Martin [31, 32], which includes the losses within the metals. The overall resonance strength of the entire Fano system is given by the product of the superradiant resonance oscillator strength modulated by the Fano–like asymmetric line shape:

$$\sigma_t(\omega) = \frac{a^2}{\left(\frac{\omega^2-\omega_s^2}{2W_s\omega_s}\right)^2+1} \cdot \frac{\left(\frac{\omega^2-\omega_a^2}{2W_a\omega_a}+q\right)^2+b}{\left(\frac{\omega^2-\omega_a^2}{2W_a\omega_a}\right)^2+1} \quad (1)$$

In this formula, a is the maximum amplitude of the super-radiant resonance, ω_s and W_s are the resonance frequency and spectral width for the superradiant resonance, respectively; ω_a and W_a are the resonance energy position and spectral width of the asymmetric Fano resonance; q is the asymmetry parameter, and b is the modulation damping parameter related to intrinsic losses. The fitted values of q and b as a function of the gap size and offset are shown in Figures 3c and 3d, respectively. The modulation parameter b, defined as the ratio of the heat energy lost in the metallic

structure to the energy that is transferred from the bright mode to the dark mode, exhibits a similar monotonic increase as both the gap g and offset Δs increase. There is a concomitant reduction in the absolute value of the asymmetry parameter q as the coupling between the two pairs grows weaker. We also observe that the values of q and b in Figure 3d change more quickly than in Figure 3c, which implies that the Fano resonance is more sensitive to offsetting in this 3D system. It is noteworthy that the line shape of Fano resonance is also essentially determined by the intrinsic damping in the metal, in addition to the structural parameters. Reducing or compensating the losses [33, 34] in the metal is an alternative method to achieve stronger Fano resonances.

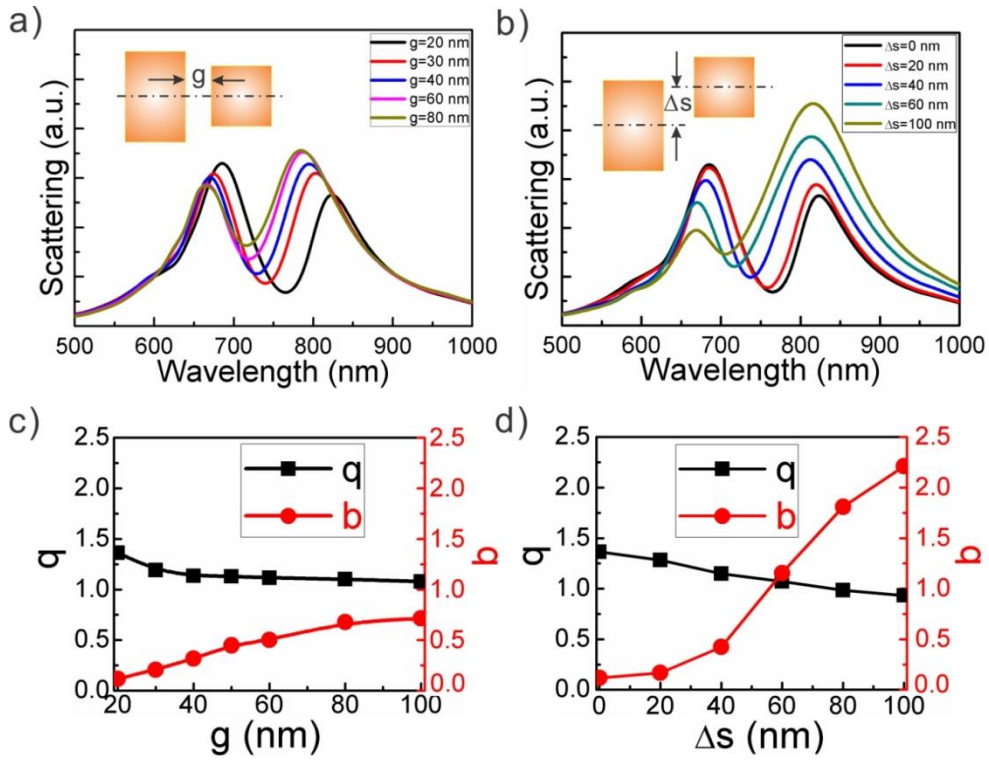

Fig. 3 (a) Calculated scattering spectra versus gap g. (b) Scattering spectra versus offset Δs , the gap is fixed at 20 nm. In (a) and (b), Geometry setting: l_1 = 120 nm, w_1 = 80 nm, l_2 = 80 nm, w_2 = 80 nm, and t = 20 nm. All modelled structures are embedded in an effective dielectric medium with a refractive index of 1.25. The insets show a vertical view of the Fano resonance system. (c) and (d) Asymmetry parameter q and modulation damping parameter b as a function of the gap g and offset Δs , respectively.

The TFL nanostructures can serve as a highly efficient nanoscale sensor, because the corresponding Fano resonances are particularly sensitive to the adjacent media, and because the

spectra are with relatively narrow linewidths. Figure 4(a) shows the calculated scattering spectra of the TFL nanostructures placed on a glass substrate and covered by media of different refractive indices. The Fano resonance exhibits a very pronounced red-shift with increasing refractive index of the surrounding medium. The sensitivity of the system, defined as the shift of the resonance wavelength (Fano minimum) per unit change of the refractive index, is 372 nm/RIU, as shown in Fig 4(b). Furthermore, the figure of merit (FOM) defined as the shift in Fano resonance energy divided by the resonance linewidth [19], namely $(\Delta E/\Delta n)$/(linewidth), is also introduced. In our case, the FOM is 6.06, which is not only greater than those measured for individual gold and silver nanoparticles [35], but is also greater than both the experimental FOM value (5.7) and the theoretical value (5.1) of the well-known heptamer structures with strong Fano resonances [21].

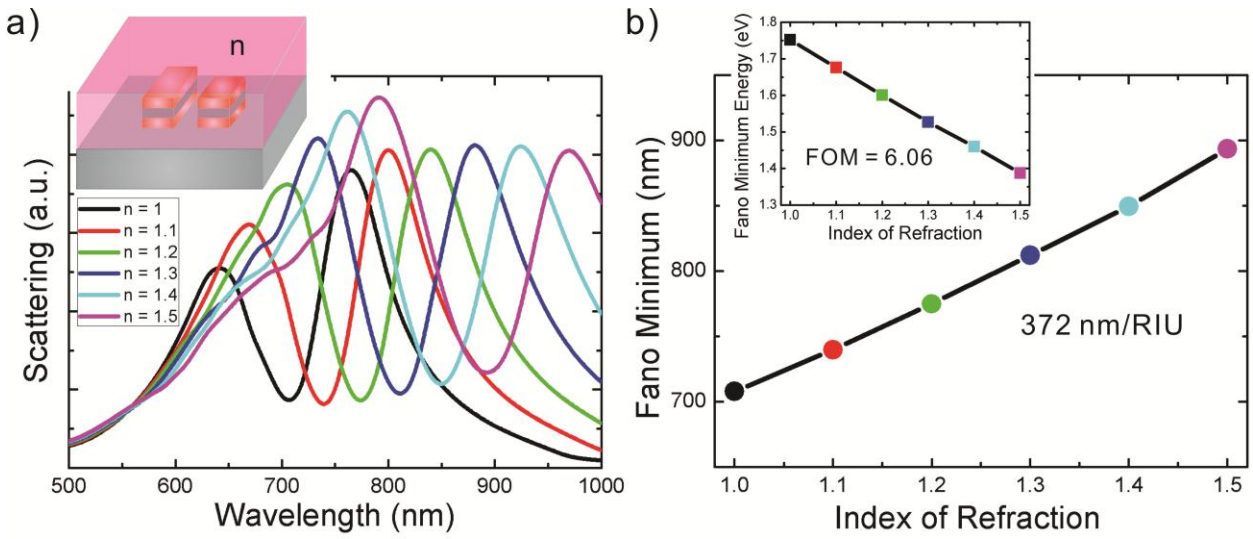

Fig. 4 (a) Calculated scattering spectra of the TFL structure in different dielectric environments. The TFL structure is placed on a glass substrate of refractive index 1.5. A sketch of the modelled structures is shown in the inset. Geometry setting: l_1 = 120 nm, w_1 = 80 nm, l_2 = 80 nm, w_2 = 80 nm, t = 20 nm, d = 20 nm, and g = 20 nm. (b) Plot of the Fano minimum wavelength as a function of the refractive index of the local medium. The inset shows the energy shifts of the plasmon resonances versus the index of refraction.

In conclusion, we have investigated the effect of symmetry breaking on a 3D plasmonic cut-wire quadrumer. A simple plasmonic structure composed of two different-sized cut-wire pairs has been proposed and demonstrated to exhibit Fano resonance characteristics. It has been shown experimentally that the Fano resonances can be adjusted by simply changing the length of the cut-wire pair. By fitting the scattering spectra for different geometrical sizes to a general equation derived in Ref. [32], we have retrieved the asymmetry parameter q and the modulation damping parameter b, which quantitatively describe the near-field coupling in the Fano resonance system. From our Comsol modelling results and analysis, we find that the Fano resonance can be precisely tuned using both the gap and the offset between the two cut-wire pair units. In addition, this 3D Fano resonance system acts as an efficient electromagnetic energy cavity, and can store significant optical energy. The 3D structure developed in this paper provides a meaningful supplement to the plasmonic Fano resonance system family, and these results may facilitate applications in plasmonic lasers, sensing, thin film solar cells and metamaterials.

Supporting Information

Additional details on electric field intensity enhancement, scattering spectra as a function of incidence angle, and modelled scattering spectra as a function of the cut-wire length under normal illumination condition.

Acknowledgements

Access to the Melbourne Centre for Nanofabrication (MCN) under the Technology Fellowships program is gratefully acknowledged. P.M. thanks the ARC for support under LF Grant 100100117. X.W. thanks Dr. Steven J. Barrow of School of Chemistry and Bio21 Institute for assistance with dark field microscopy, and also Dr. Zoran Vasić and Dr. Sean Langelier of the MCN for training on the electron beam evaporator. X.W. thanks Dr. Kevin Tatur for advice on the spectral fitting algorithm.

REFERENCES

(1) N. I. Zheludev, S. L. Prosvirnin, N. Papasimakis, V. A. Fedotov, *Nat. Photonics* 2008, **2**, 351–354.

(2) A. E. Nikolaenko, F. De Angelis, S. A. Boden, N. Papasimakis, P. Ashburn, E. Fabrizio, N. I. Zheludev, *Phys. Rev. Lett*. 2010, **104**, 153902.

(3) T. Zentgraf, A. Christ, J. Kuhl, H. Giessen, *Phys. Rev. Lett*. 2004, **93**, 243901.

(4) S. Zhang, D. A. Genov, Y. Wang, M. Liu, X. Zhang, *Phys. Rev. Lett*. 2008, **101**, 047401.

(5) N. Liu, T. Weiss, M. Mesch, L. Langguth, U. Eigenthaler, M. Hirscher, C. Sonnichsen, H. Giessen, *Nano Lett*. 2010, **10**, 1103–1107.

(6) V. A. Fedotov, M. Rose, S. L. Prosvirnin, N. Papasimakis, N. I. Zheludev, *Phys. Rev. Lett.* 2007, **99**, 147401.

(7) B. Luk'yanchuk, N. I. Zheludev, S. A. Maier, N. J. Halas, P. Nordlander, H. Giessen, C. T. Chong, *Nat. Mater*. 2010, **9**, 707–715.

(8) M. Z. Liu, T.-W. Lee, S. K. Gray, P. Guyot-Sionnest, M. Pelton, *Phys. Rev. Lett*. 2009, **102**, 107401.

(9) S. A. Maier, P. G. Kik, H. A. Atwater, S. Meltzer, E. Harel, B. E. Koel, A. A. G. Requicha, *Nat. Mater*. 2003, **2**, 229-232.

(10) K. A. Tetz, L. Pang, Y. Fainman, *Opt. Lett*. 2006, **31**, 1528–1530.

(11) C. Y. Chen, I. W. Un, N. H. Tai, T. J. Yen, *Opt. Express* 2009, **17**, 15372–15380.

(12) S. Mukherjee, H. Sobhani, J. B. Lassiter, R. Bardhan, P. Nordlander, N. J. Halas, *Nano Lett*. 2010, **10**, 2694–2701.

(13) N. Verellen, Y. Sonnefraud, H. Sobhani, F. Hao, V. V. Moshchalkov, P. Van Dorpe, P. Nordlander, S. A. Maier, *Nano Lett*. 2009, **9**, 1663–1667.

(14) B. Gallinet, O. J. F. Martin, *Opt. Express* 2011, **19**, 22167−22175.

(15) V. Giannini, Y. Francescato, H. Amrania, C. C. Phillips, S. A. Maier, *Nano Lett*. 201**1**, **11**, 2835−2840.

(16) L. V. Brown, H. Sobhani, J. B. Lassiter, P. Nordlander, N. J. Halas, *ACS Nano* 2010, **4**, 819–832.

(17) F. Hao, P. Nordlander, Y. Sonnerfraud, P. Van Dorpe, S. A. Maier, *ACS Nano* 2009, **3**, 643–652.

(18) Y. Sonnefraud, N. Verellen, H. Sobhani, G. A. E. Vandenbosch, V. V. Moshchalkov, P. Van Dorpe, P. Nordlander, S. A. Maier, *ACS Nano* 2010, **4**, 1664–1670.

(19) J. A. Fan, K. Bao, C. Wu, J. Bao, R. Bardhan, N. J. Halas, V. N. Manoharan, G. Shvets, P. Nordlander, F. Capasso, *Nano Lett*. 2010, **10**, 4680–4685.

(20) J. A. Fan, C. H. Wu, K. Bao, J. M. Bao, R. Bardhan, N. J. Halas, V. N. Manoharan, P. Nordlander, G. Shvets, F. Capasso, *Science* 2010, **328**, 1135–1138.

(21) J. B. Lassiter, H. Sobhani, J. A. Fan, J. Kundu, F. Capasso, P. Nordlander, N. J. Halas, *Nano Lett*. 2010, **10**, 3184–3189.

(22) M. Hentschel, M. Saliba, R. Vogelgesang, H. Giessen, A. P. Alivisatos, N. Liu, *Nano Lett*. 2010, **10**, 2721–2726.

(23) M. Hentschel, D. Dregely, R. Vogelgesang, H. Giessen, N. Liu, *ACS Nano* 2011, **5**, 2042-2050.

(24) N. Liu, L. Langguth, T. Weiss, J. Kastel, M. Fleischhauer, T. Pfau, H. Giessen, *Nat. Mater*. 2009, **8**, 758–762.

(25) N. Liu, M. Hentschel, T. Weiss, A. P. Alivisatos, H. Giessen, *Science* 2011, **332**, 1407–1410.

(26) T. J. Davis, M. Hentschel, N. Liu, H. Giessen, *ACS Nano* 2012, **6**, 1291−1298.

(27) G. Dolling, M. Wegener, S. Linden, *Opt. lett.* 2007. **32**, 551-553.

(28) P. B. Johnson, R. W. Christy, *Phys. Rev. B* 1972, **6**, 4370.

(29) J. Kottmann, O. Martin, *Opt. Lett*. 2001, **26**, 1096-1098.

(30) J. A. Fan, K. Bao, J. B. Lassiter, J. Bao, N. J. Halas, P. Nordlander, F. Capasso, *Nano Lett*. 2012, **12**, 2817-2821.

(31) B. Gallinet, O. J. F. Martin, *Phys. Rev. B* 2011, **83**, 235427.

(32) B. Gallinet, O. J. F. Martin, *ACS Nano* 2011, **5**, 8999-9008.

(33) M. C. Gather, K. Meerholz, N. Danz, K. Leosson, *Nat. Photonics* 2010, **4**, 457.

(34) J. Grandidier, G. Colas des Francs, S. Massenot, A. Bouhelier, L. Markey, J.-C. Weeber, C. Finot, A. Dereux, *Nano Lett*. 2009, **9**, 2935.

(35) H. W. Liao, C. L. Nehl,. J. H. Hafner, *Nanomedicine* 2006, **1**, 201–208.